

The Size Distribution of the Agitated Saline Microbubbles for c-TCD generated using Standard Manual Methods

zhengbin Pan¹, Yiting Xiao¹, Zhiyue Wang¹, Bo Kong¹, and Yiyi Liang²

¹Guangdong Technion-Israel Institute of Technology Department of Chemical Engineering

²Guangdong Provincial People's Hospital

June 8, 2023

Abstract

Agitated saline microbubbles (MBs) is a common contrast agent for determining right-to-left shunt (RLS) by the contrast Transcranial Doppler (c-TCD). The size of the generated bubbles is not standardized in clinical practice. The microbubbles were generated using the recommended manual method by reciprocating motion through two syringes. The bubble size distributions (BSD) were measured using the microscopic shadow imaging technique. The results show that the diameter of MBs is mainly distributed between 10-100 μm , the mean bubble size is between 21-34 μm , the Sauter mean diameter (D_{32}) is mainly between 50-300 μm , and the standard deviation (SD) is between 6-17 μm in 60 experiments. It provides a more accurate basis for the recommended manual method instability. The high variance values of the BSD indicate that the manual method has low stability and repeatability. The results of this study can be useful for further improvement of the reliability of c-TCD in detecting RLS.

Research Highlights This study provided the first detailed descriptions of the size distribution of microbubbles in a flowing contrast agent by the microscopic shadow imaging technique. It reveals significant differences in the bubble size of manual foaming during repeated manipulations for each individual and between individuals.

The Size Distribution of the Agitated Saline Microbubbles for c-TCD generated using Standard Manual Methods

Zhengbin Pan¹, Yiting Xiao¹, Zhiyue Wang¹, Bo Kong^{1*}, Yiyi Liang^{2*}

¹ Department of Chemical Engineering, Guangdong Technion-Israel Institute of Technology (GTIIT), 241 Daxue Road, Shantou 515063, China

² Department of Neurology, Guangdong Neuroscience Institute, Guangdong Provincial People's Hospital (Guangdong Academy of Medical Sciences), Southern Medical University Guangzhou 510080, China

*Correspondence authors:

Email: bo.kong@gtiit.edu.cn (Bo Kong); ldaisy19@163.com (Yiyi Liang)

Abstract

Agitated saline microbubbles (MBs) is a common contrast agent for determining right-to-left shunt (RLS) by the contrast Transcranial Doppler (c-TCD). The size of the generated bubbles is not standardized in clinical practice. The microbubbles were generated using the recommended manual method by reciprocating motion through two syringes. The bubble size distributions (BSD) were measured using the microscopic shadow imaging technique. The results show that the diameter of MBs is mainly distributed between 10-100 μm , the mean bubble size is between 21-34 μm , the Sauter mean diameter (D_{32}) is mainly between 50-300 μm , and the standard deviation (SD) is between 6-17 μm in 60 experiments. It provides a more accurate basis for the recommended manual method instability. The high variance values of the BSD indicate that the manual

method has low stability and repeatability. The results of this study can be useful for further improvement of the reliability of c-TCD in detecting RLS.

Research Highlights

This study provided the first detailed descriptions of the size distribution of microbubbles in a flowing contrast agent by the microscopic shadow imaging technique. It reveals significant differences in the bubble size of manual foaming during repeated manipulations for each individual and between individuals.

Keywords Microbubbles; Bubble size distributions; Manual; Repeatability

Introduction

Foramen ovale is a physiological channel of the atrial septum during the embryonic period. After birth, the primary and secondary septum get close to each other, adhere to each other, and gradually fuse to form a permanent atrial septum **(1)**. Suppose the fusion is not complete after three years of age. In that case, the remaining fissure-like channel is called patent foramen ovale (PFO), the most common congenital heart abnormality in adults **(2 - 4)**. PFO patients may suffer from low blood oxygen levels and cryptogenic strokes (CS), leading to serious health issues. **(5)**. Neurologists and cardiologists have become increasingly aware of the symptoms in recent years, and many hospitals have launched different examination programs.

For detecting PFO, three ultrasound techniques have been developed: transesophageal echocardiography (TEE) **(6, 7)**, "gold standard" contrast-transthoracic echocardiography (c-TTE) **(8, 9)**, and contrast-transcranial doppler (c-TCD) **(6)**. By contrast, c-TCD offers a sensitive, easy-to-perform, non-invasive method for assessing the presence of RLS in the patient's heart **(10, 11)**. The c-TCD method produces less discomfort for the patients during the test, and it is a useful initial screening tool in determining whether a patient has RLS. Microbubbles are used as contrast agents in the c-TCD test, which are prepared by mixing the isotonic saline solution with air, which is injected into a cubital vein for the test. In the presence of a right-to-left shunt, the air-containing echo contrast agent will bypass pulmonary circulation and induces microembolic signals in the basal cerebral arteries **(12)**. Nowadays, saline contrast use has been applied to enhance intracardiac navigation and is recognized as an effective kind of contrast agent when applying c-TCD for diagnosing PFO **(13 - 15)**. Importantly, many problems in this detection process still lead to missed diagnoses, which still needs further in-depth research. For example: changing the contrast agent **(16)**, changing the intravenous catheters **(17)**, improving the Valsalva action **(18)**, and so on, but there are few studies on the generation of microbubbles.

The behavior of microbubbles in venous blood is of great importance for testing accuracy. The microbubbles' size has been shown to affect their longevity and acoustic behavior significantly **(19)**. After infusion of contrast agent, microbubbles can circulate throughout the body, and the size of the bubbles determines their lifespan and performance after entering the blood circulation. Large bubbles cannot pass through capillaries, while small air bubbles have a poor scattering effect on ultrasound **(20)**. In addition, the size of the bubble diameter is also related to tissue penetration because the Laplace pressure and blood pressure effects will further affect the lifetime of the microbubbles **(21)**.

Therefore, the size of microbubbles plays a significant role in c-TCD as the contrast media for diagnosing PFO. The recommended manual procedure for generating MBs is mixing 9ml isotonic saline solution and 1ml air with a three-way stopcock by exchange of saline/air mixture between the syringes and injecting the generated MBs into the subject through the cubital vein as a bolus **(22)**. Relevant studies are less available on the MBs generated by this method, especially on the BSD and repeatability of the BSD.

Herein, we performed a detailed measurement of the BSD to provide reliable and useful data for the future enhancement of c-TCD. For the first time, a microscopic shadow imaging technique was used to observe and record the MBs generated with the manual methods, then MBs were subjected to detailed physical characterization. The overarching aim of the research was to obtain the BSD data and characterize how much variation there is in c-TCD practice.

Materials and Methods

The study was approved by the Guangdong Provincial People’s Hospital (Guangdong Academy of Medical Sciences). All of the data were acquired after obtaining authors permission.

The microbubbles were generated through standard reciprocating manual operation and measured with the microscopic shadow image technique. The details are as follows:

Preparation of the agitated saline microbubbles

The preparation of microbubbles is shown in Figure 1a. The experiment was carried out by hand pushing the syringe plunger reciprocating motion to create microbubbles. Each operator in each repeated experiment uses a 10 ml injector to extract 9 ml of 0.9% saline solution from the infusion bottle, then extract 1 ml of air. Then, each syringe plunger was pushed forward and backward ten times (Overall reciprocating motion 20 times) to mix the air with saline solution to activate the contrast agents **(23)**. Finally, the operator quickly and manually switched the three-way stopcock, injecting the saline-bubble mixture (within 1-2 seconds) into the flow test section. At the same time, the high-speed camera (Figure 1b) started taking images immediately. Six volunteers (M-1, M-2, M-3, M-4, M-5, and M-6) took part in the experiment, each completing ten repeated operations.

Microscopic shadow imaging technique

The size of the microbubbles was measured using a microscopic shadow imaging technique. As indicated in Figure 2a, the sketch of the imaging system shows a CMOS-Camera (Nova S12 Photron LaVision) with a resolution of 1024 by 1024 pixels, a Zeiss stereo microscope (SteREO Discovery V12 Zeiss LaVision), a flow test section, and an LED light (VI - Strobe LED 120W V2 Lavisision Germany). The MBs could stagnate on the top wall of the test section due to the buoyancy effect during the experiments when the test section is placed horizontally, which would block the camera. Therefore, the flow test section was placed vertically in the experiments at the lens’s focal length, 8 mm, and the Zeiss stereo microscope and CMOS camera were placed in a horizontal configuration. An LED light was fixed behind the flow test section, and a Fresnel lens collated the light source to illuminate the test section. The optical platform was equipped with a motorized x-y table, and adjustment of the focal length was controlled by Davis software (Lavisision Germany) and a joystick.

The flow test section was made into a flat structure so that less light reflection would occur, which was constructed with two transparent Plexiglass (PMMA) with dimensions of $100 \times 100 \times 1$ mm (Length \times Width \times Thickness) and a stainless steel plate of the same size with a flow channel in the middle. The length and width of the flow channel are designed to be 2 mm and 50 mm, respectively, and manufactured by laser cutting. To better conform to the operation of the TCD, an inlet hose with a diameter close to the 18 G venous retention needle was used **(17)**. The details of the flow test section are depicted in Figure 2b. Finally, the third outlet of the three-way stopcock was connected to the flow test section inlet.

Recording and processing of microbubbles

In the current setting, these bubbles in images were magnified by a Zeiss stereo microscope lens assembly achieving $50 \times$ optical magnification with a depth of field of $86 \mu\text{m}$, the lateral spatial resolution is 2.00 mm, and the vertical resolution is 2.45 mm. In order to obtain accurate statistics, a total of 1600 images in each measurement were collected. The images were post-processed and analyzed using the software Davis (Lavisision Germany). First, the original image was normalized and noise-filtered, and then particle detection with binarization was performed. The parameters for image processing and particle recognition can be set in the Analyzer settings panel, and the parameters are summarized in Table 1.

Results and discussion

The examples of MBs analysis are shown in Figure. 3, the difference in diameter of bubbles in the focal length range can be seen, and bubbles range in diameter from about $10 \mu\text{m}$ to $200 \mu\text{m}$. Throughout the whole process of analysis of the video, the shape of the bubbles is regular. It is clear that the majority of

the bubbles were spherical owing to the surface tension. To understand the effect of different test times on the number of bubbles, we studied the bubbles captured in each set of 1600 images. Figure 4 shows a large difference in the density of bubbles in every experiment. Comparing the average density of bubbles calculated for each group of 10 experiments, the maximum difference in the number density of captured bubbles is about $150,000/\text{cm}^3$, indicating that the manual reciprocating motions greatly impact the number of bubbles produced.

Figure 5 displays the statistical histograms of the BSD in two example operations, showing that the bubble size distribution is very close to the log-normal distribution, which is a feasible model used to describe the microbubble size distribution in the experiment. The expression for log-normal distribution is shown as follows (24) :

Hosted file

image1.emf available at <https://authorea.com/users/627048/articles/648141-the-size-distribution-of-the-agitated-saline-microbubbles-for-c-tcd-generated-using-standard-manual-methods>

(1)

Hosted file

image2.emf available at <https://authorea.com/users/627048/articles/648141-the-size-distribution-of-the-agitated-saline-microbubbles-for-c-tcd-generated-using-standard-manual-methods>

(2)

Hosted file

image3.emf available at <https://authorea.com/users/627048/articles/648141-the-size-distribution-of-the-agitated-saline-microbubbles-for-c-tcd-generated-using-standard-manual-methods>

(3)

The log-normal distribution uses the following parameters,

μ : mean of the natural logarithm of the data.

σ : standard deviation of the natural logarithm of the data.

The BSDs of the MBs generated by each manual operation ten times are shown in Figure 6 (a, b, c, d). The results indicate that the size distribution of microbubbles varied with the number of operations, especially between 20-60 μm . The diameter of the bubbles is mainly distributed in the range of 10-100 μm , with a wide distribution range. These bubbles may affect the detection results of c-TCD after entering the vein because the lifetime of the bubbles decreases as the bubble size decreases, and large bubbles cannot pass through the capillaries and fail to reach the foramen ovale. Eventually, the inhomogeneous mixture of gas-liquid will cause hemodynamic changes.

Figure 7a compares the bubble size distribution averaged of 10 experiments performed by each person, with the curves being messy between 15-80 μm , which also shows that the difference in results between each individual is particularly obvious. In addition, the mean bubble size, Sauter mean diameter, and standard deviation value of 10 manual operations for each volunteer are shown graphically in Figure 7(b, c, and d). As can be seen, the reproducibility is relatively poor. The mean bubble size is between 21-34 μm , the D_{32} is mainly between 50-300 μm , and the maximum standard deviation was close to 17 μm in 60 experiments. This initial inference has been strongly validated that the velocity and strength of each manual operation vary when pushing with the syringe leading to this phenomenon, especially between individuals. Through the analysis of Figure 7 and Table 2, the results show that the stronger the gas-liquid mixing, the more

uniform the state, and the mean bubble size and standard deviation of the bubbles may decrease. These values are unstable with large fluctuations, which provides a more accurate basis for the instability of the manual method.

Conclusions

This study measured the BSD of MBs generated with the recommended manual method using the microscopic shadow imaging technique. The MBs generated by the different operators were pushed through a transparent flow test section, and their images were taken by a microscope and a camera. After processing and analyzing the images, the BSD of the MBs was obtained. The data show that the diameter of MBs is mainly distributed between 10-100 μm , the mean bubble size is between 21-34 μm , the D_{32} is mainly between 50-300 μm , and the standard deviation is between 6-17 μm in 60 experiments. The data revealed the differences in the size distribution of manual operation bubbles for the different operators with different strengths. These findings are important for the future development of c-TCD. In our future work, the influence of different bubble sizes on the accuracy of c-TCD will be studied. A more suitable MBs generation procedure or device with high reliability will be developed to replace human manual operation in our future studies.

Acknowledgements

Funding

Shantou Science and Technology Bureau (200909094890694)

We express our appreciation to Xiaoyu Chen, Liling Cai, Yujie Zhang and Qianyue Jian for their help during experimental work. This work was supported by the Shantou Science and Technology Bureau (200909094890694).

Abbreviations

MBs microbubbles

RLS right-to-left shunt

PFO patent foramen ovale

CS cryptogenic strokes

c-TCD contrast-transcranial Doppler

TEE transesophageal echocardiography

c-TTE contrast-transthoracic echocardiography

BSD bubble size distributions

D_{32} Sauter mean diameter

SD standard deviation

Reference:

1. Zoghbi W A. Patent foramen ovale: Going beyond the bubbles. *JACC: Cardiovascular Imaging* 2014; 7: 251-253.
2. Hagen PT, Scholz DG, Edwards WD. Incidence and size of patent foramen ovale during the first 10 decades of life: an autopsy study of 965 normal hearts. *Mayo Clin Proc* 1984; 59: 17-20.
3. Ailani J. Migraine and patent foramen ovale. *Current neurology and neuroscience reports* 2014; 14: 1-5.
4. Kutty S, Sengupta P P, Khandheria B K. Patent foramen ovale: the known and the to be known. *Journal of the American college of cardiology* 2012; 59: 1665-1671.

5. Lechat P H, Mas J L, Lascault G, et al. Prevalence of patent foramen ovale in patients with stroke. *New England Journal of Medicine* 1988; 318: 1148-1152.
6. Mojadidi M K, Gevorgyan R, Tobis J M. A comparison of methods to detect and quantitate PFO: TCD, TTE, ICE and TEE. *Patent foramen ovale* 2015; 55-65.
7. Daniel W G, Mügge A. Transesophageal echocardiography. *New England Journal of Medicine* 1995; 332: 1268-12100.
8. Marriott K, Manins V, Forshaw A, et al. Detection of right-to-left atrial communication using agitated saline contrast imaging: experience with 1162 patients and recommendations for echocardiography. *Journal of the American Society of Echocardiography* 2013; 26: 96-102.
9. Mojadidi M K, Winoker J S, Roberts S C, et al. Accuracy of conventional transthoracic echocardiography for the diagnosis of intracardiac right-to-left shunt: a meta-analysis of prospective studies. *Echocardiography* 2014; 31: 1036-1048.
10. Spencer M P, Moehring M A, Jesurum J, et al. Power m-mode transcranial Doppler for diagnosis of patent foramen ovale and assessing transcatheter closure. *Journal of Neuroimaging* 2004; 14: 342-349.
11. Fu J, Hui P, Ding Y, et al. Feasibility of evaluating right-to-left shunt by contrast-enhanced transcranial Doppler. *Chinese Journal of Medical Ultrasound (Electronic Edition)* 2020; 17: 255
12. Webb G, Gatzoulis M A. Atrial septal defects in the adult: recent progress and overview. *Circulation* 2006; 114: 1645-1653.
13. Ziskin MC, Bonakdarpour A, Weinstein DP, Lynch PR. Contrast agents for diagnostic ultrasound. *Invest Radiol* 1972; 7: 500-5.
14. Waggoner AD, Barzilai B, Perez JE. Saline contrast enhancement of tricuspid regurgitant jets detected by Doppler color flow imaging. *Am J Cardiol* 1990; 65: 1368-71.
15. Woods TD, Patel A. A critical review of patent foramen ovale detection using saline contrast echocardiography: when bubbles lie. *J Am Soc Echocardiogr* 2006; 19: 215-22.
16. Lange MC, Zetola VF, Piovesan EJ, et al. Saline versus saline with blood as a contrast agent for right-to-left shunt diagnosis by transcranial Doppler: Is there a significant difference? *Journal of Neuroimaging* 2012; 22: 17-20.
17. Khan K A, Yeung M, Shuaib A. Comparative study of 18 gauge and 20 gauge intravenous catheters during transcranial Doppler ultrasonography with saline solution contrast. *Journal of ultrasound in medicine*,1997; 16: 341-344.
18. Droste DW, Kriete JU, Stypmann J, et al. Contrast transcranial Doppler ultrasound in the detection of right-to-left shunts: Comparison of different procedures and different contrast agents. *Stroke*,1999, 30: 1827-1832
19. Jangjou A, Meisami A H, Jamali K, et al. The promising shadow of microbubble over medical sciences: from fighting wide scope of prevalence disease to cancer eradication. *Journal of Biomedical Science* 2021; 28: 1-24.
20. Kabalnov A, Klein D, Pelura T, et al. Dissolution of multicomponent microbubbles in the bloodstream: 1. Theory. *Ultrasound in medicine & biology* 1998; 24: 739-749.
21. Samiotaki G, Vlachos F, Tung Y S, et al. A quantitative pressure and microbubble-size dependence study of focused ultrasound-induced blood-brain barrier opening reversibility in vivo using MRI. *Magnetic resonance in medicine* 2012; 67: 769-777.
22. Nedeltchev K, Mattle H P. Contrast-enhanced transcranial Doppler ultrasound for diagnosis of patent foramen ovale. *Handbook on neurovascular ultrasound* 2006; 21: 206-215.

23. Wang Y, Zeng J, Yin L, et al. Modified Right Heart Contrast Echocardiography Versus Traditional Method in Diagnosis of Right-to-Left Shunt: A Comparative Study. Polish Journal of Radiology 2016; 81: 428.

24. Devore J L. Probability and Statistics for Engineering and the Sciences. Cengage learning 2011.

Tables

Table 1. Parameters of the Experiments of image preprocessing and particle detection (LaVision)

Parameter	Description	Value
Normalization radius	Strength of the maximum sliding filter, expressed as the search radius in pixels. A smaller value concentrates on small-scale features. A larger value conserves global structures.	75 pixels
Reduce pixel noise	Denosing filter with a certain smoothing radius	weak
Binarization threshold	The percentage intensity level of the normalized image at which the intensity is split between black (=shadow) and white (=background).	50 %
Minimum shadow area	The minimum number of pixels the particle shadow must contain to be accepted in the list.	25 pixels
Minimum slope	A filter for the minimum sharpness of the image, defined as the relative drop of intensity (=slope) at the particle rim.	3 %

Table 2. The microscopic shadow imaging analysis.

	M-1	M-1	M-2	M-2	M-3	M-3	M-4	M-4	M-5	M-5	M
	Mean	SD	M								
	(μm)										
1	26.53	10.51	29.50	13.10	27.49	10.77	24.67	8.74	31.58	14.21	2
2	25.94	9.89	28.77	10.40	25.02	9.17	26.90	9.54	31.55	14.43	2
3	26.23	9.96	29.22	12.32	27.90	10.25	24.55	8.52	33.23	15.91	2
4	24.87	9.04	28.00	11.12	27.13	10.78	25.09	9.15	31.43	13.85	2
5	23.90	8.00	26.67	10.42	26.15	9.99	23.91	8.09	34.09	16.38	2
6	23.86	8.01	29.94	13.44	25.07	8.85	25.51	8.76	33.27	15.72	2
7	25.51	9.13	29.54	13.43	26.28	10.28	26.12	9.53	33.26	16.39	2
8	25.21	9.47	29.13	12.56	28.78	11.75	24.41	8.26	32.89	16.09	2
9	28.06	9.45	29.33	10.35	28.53	11.90	24.09	8.04	29.73	12.99	2
10	28.46	10.48	27.33	10.98	27.45	10.80	24.35	8.40	30.43	13.57	2

Figure Captions List

Figure 1. (a) The schematic diagram of the standard manual operation; (b) Microbubbles generated by standard manual methods

Figure 2. (a) The sketch of the imaging system; (b) The flow test section

Figure 3. The images of microbubbles captured under the standard manual operation

Figure 4. The number density of bubbles under the standard manual operation

Figure 5. The statistical histograms of the BSD manual operation: (a) M-1; (b) M-2

Figure 6. Effect of different standard manual operations on BSD: (a) bubbles generated by M-1; (b) bubbles generated by M-2; (c) bubbles generated by M-3; (d) bubbles generated by M-4

Figure 7. Reproducibility of (a) The BSD averaged about M-1, M-2, M-3, M-4, M-5, and M-6, respectively; (b) mean bubble size measurements; (c) the Sauter mean bubble diameters; (d) bubble size standard deviations

Figure 1

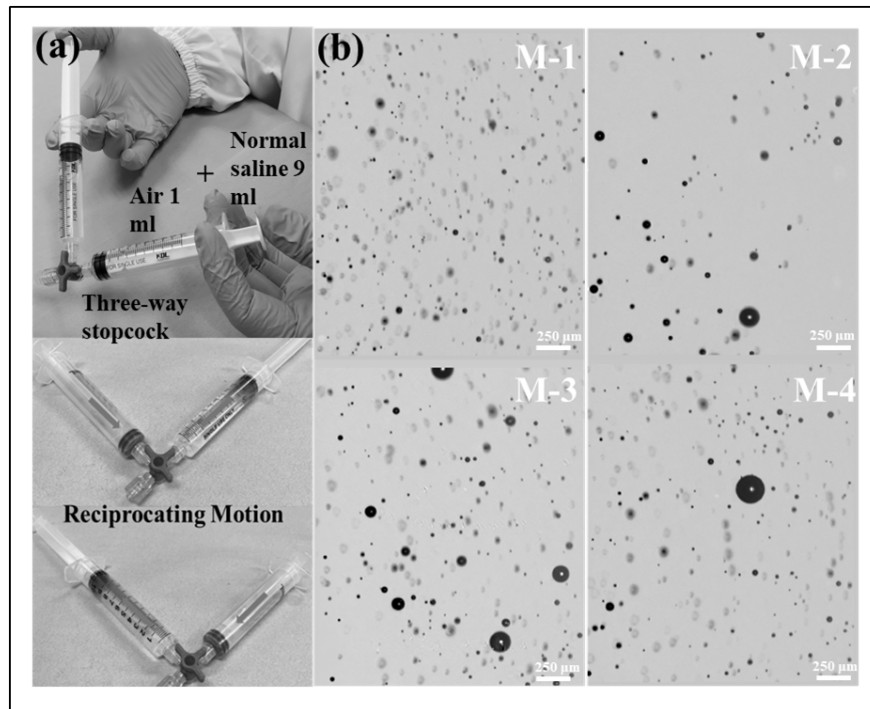


Figure 2

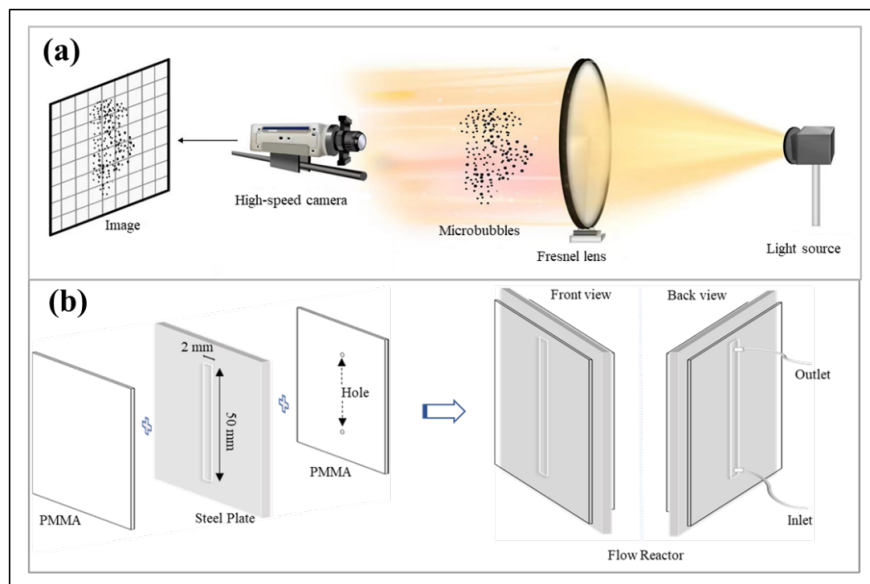


Figure 3

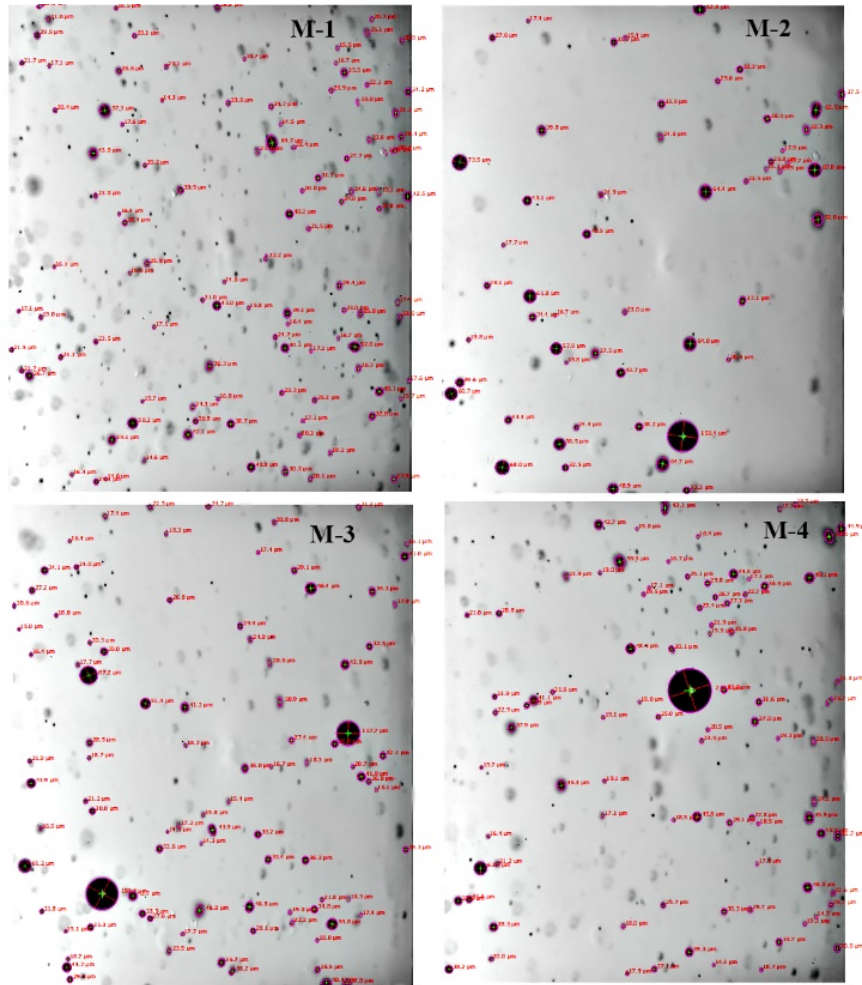


Figure 4

Figure 5

Figure 6

Figure 7

Hosted file

Recording of microbubbles.mp4 available at <https://authorea.com/users/627048/articles/648141-the-size-distribution-of-the-agitated-saline-microbubbles-for-c-tcd-generated-using-standard-manual-methods>